Fatigue properties and fracture mechanism of load carrying type fillet joints with one-sided welding

Takamasa Abe
Kobelco Construction Machinery CO.,LTD, Japan
abe.takamasa@kobelco.com

Hiroyuki Akebono, Masahiko Kato, Atsushi Sugeta
Department of Mechanical Science and Engineering, Hiroshima University, Japan
akebono@hiroshima-u.ac.jp, mkato@hiroshima-u.ac.jp, asugeta@hiroshima-u.ac.jp

ABSTRACT. The structures of the hydraulic excavator and the crane have numerous one-sided welded joints. However, attachments with box like structures are difficult to weld at both sides. Therefore, high accurate evaluation method is needed. In this study, the fatigue properties and the fracture mechanism of the load carrying type fillet joints with one-sided welding were investigated experimentally to evaluate its fatigue damage with high accuracy based on the experimental results. As the results, fatigue cracks in the test piece initiated from the tip of the unwelded portion and propagated into the welding materials. Multiple welding defects were observed in the unwelded portion, but did not appear to be crack origins. Although these welding defects affected the direction of crack propagation they exerted minimal influence. The three-dimensional observations revealed that fatigue cracks initiate at an early stage of the fatigue development. We infer that the fatigue lifetime is chiefly governed by the crack propagation lifetime. Cracks were initiated at multiple sites in the test piece. As the number of cycles increased, these cracks propagated and combined. So considering the combination of cracks from multiple crack origins is important for a precise evaluation of fatigue damage.

KEYWORDS. The filet joint with One-sided welding; Crack Propagation; 3-Dimensional Observation.

INTRODUCTION

Hydraulic excavators and cranes are major heavy equipment with numerous one-sided welded joints. Although fillet weld joints are easily implemented and economical, the unwelded portion frequently initiates crack propagation. Therefore, the unwelded portion is reduced by both side welding and by adding a groove. However, attachments with box like structures are difficult to weld at both sides, and grooving cannot completely remove the unwelded portion because high-quality full penetration welds are difficult to achieve. Despite the need for an accurate evaluation method of crack propagation, the fatigue fracture mechanism and the fatigue damage in practical fillet joints with one-sided welding remains poorly understood [1 - 13]. While the fatigue strength of the unwelded portion of load-carrying cruciform-welded joints has been extensively investigated, few studies have reported on one-sided welding. Moreover, few load-carrying types are suitable for one-sided welding. Most of the existing studies evaluate the lifetime from the S-N curve and stress intensity factor, without referring to the crack development behavior. At the beginning of this study, we believed that if we could understand the crack propagation behavior in the interior structure, we would be

able to more accurately estimate the lifetime. To this end, we fabricated a test piece imitating the machine, and subjected it to fatigue tests. We also investigated the fatigue properties and fracture mechanism of a load carrying-type one-sided fillet weld by three-dimensional observation.

MATERIALS AND METHODS

Materials

The base material was high strength steel SS400 (JIS) which is used in the attachment part of a hydraulic excavator. We joined this material to the "L" shape indicated in Fig.1 by one-sided fillet welding. To prevent heat deformation of the plate during two-sided welding, we welded a grab section and stiffener plates (labeled (a) and (b), respectively, in Fig. 1) to the test piece. The welded part was cut into "L" shapes at 50mm intervals by wire cutting, excluding the welding start and end points. (see broken lines in Fig. 1). The welding rods were used equivalent material as JIS Z3313 (Wire diameter φ=1.2mm). Tab. 1, 2, and 3 give the arc welding condition, the chemical composition of the welding rods and the mechanical properties, respectively. The chemical composition and mechanical properties of SS400 are listed in Tabs. 4 and 5, respectively.

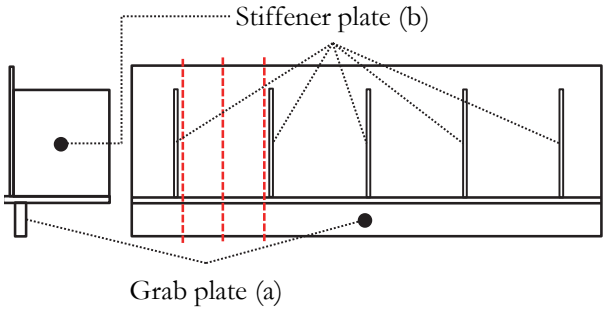

Figure 1: Manufacturing specimens.

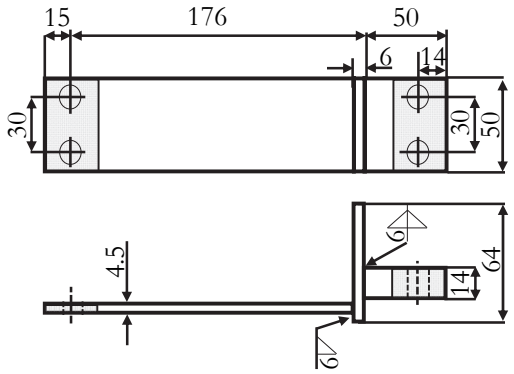

Figure 2: Shapes and dimensions of specimens.

Welding current (A)	Arc Voltage
270	31

Table1: Welding Condition.

Material	C	Si	Mn	P	S
Welding rods	0.06	0.5	1.4	0.013	0.009

Table 2: Chemical composition of welding rods [mass%].

Yield Strength σ_y (MPa)	Tensile Strength σ_B (MPa)	Elongation δ(%)	Absorbed Energy (J)
530	590	29	98

Table 3: Mechanical properties of welding rods.

Material	C	Mn	P	S
SS400	-	-	≤ 0.05	≤0.05

Table 4: Chemical composition of SS400 [mass%].

Yield Strength σ_y (MPa)	Tensile Strength σ_B (MPa)	Elongation δ(%)
245 ≤	400 ~ 510	29 ≤

Table 5: Mechanical properties of SS400.

Experimental method

The fatigue test was performed by a hydraulic servo-controlled fatigue strength-testing machine. The gray area in Fig. 2 was affixed to the jig, and the loading type of the machine was reproduced by applying a left and right cyclic load. When fixing the test piece to the jig, we also attached a strain gauge to the test piece and adjusted the test piece such that the

strain remained below 50με (the position of the strain gauge is shown in Fig. 3). The fatigue test was performed at room temperature, under the following load conditions: frequency f=20Hz, and load ratio $R_F(=F_{min}/F_{max})$=0.05. Fracture was defined as the time of complete separation of the welded joint. The fatigue test was conducted through N=10^7cycles.

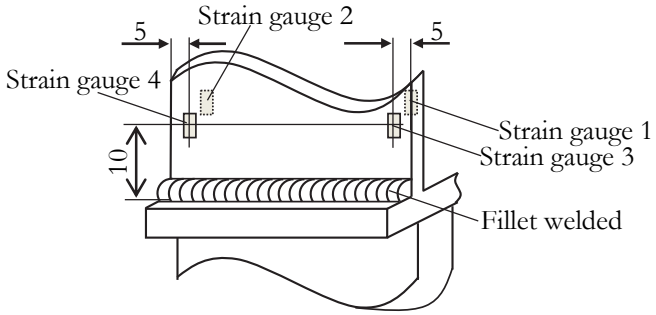

Figure 3: Position of the strain gauge near fillet weld.

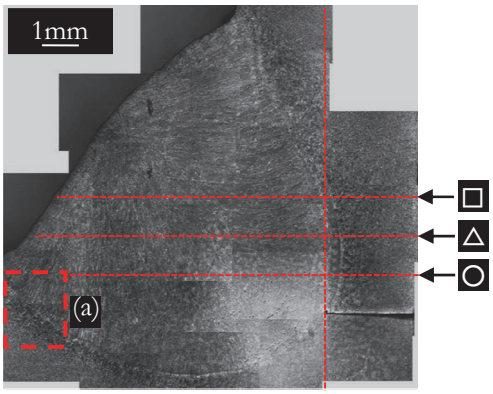

Figure 4: Microstructure observation of cross section.

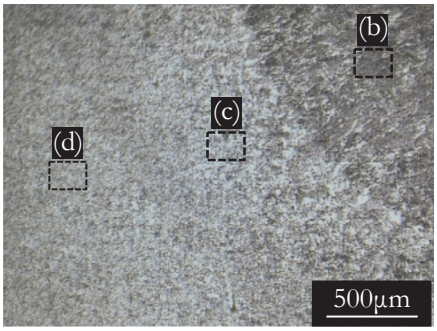

Figure 5: Microstructure observation at the material. Detail (a).

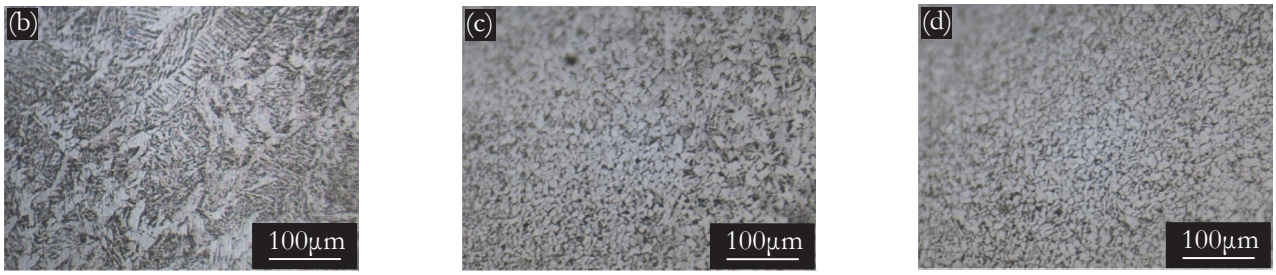

Figure 6: Microstructure observation at the material in detail.

RESULTS

Metallographic structure observation and hardness test

Fig. 4-6 show the microstructure of the one-side fillet weld zone. Three structural categories can be recognized; welding material structure, a heat affected zone, and the base material. Observations of each area reveal that the metallographic structure of the welding material had melted and solidified into a dendritic structure, and the base material has a ferrite structure. Closer to the welding metal zone, the crystal grain of the base material enlarges. The hardness results of the one-sided fillet welding are plotted in Fig. 7. The hardness was measured along the three horizontal broken lines shown in Fig. 4. The origin of the horizontal axis in Fig. 7 is the vertical line in Fig. 4, which separates the welding material (negative side) from the base material (positive side). According to Fig. 7, the welding material is 1.2 times harder than the base material. The welding material hardened because martensite was generated by the cooling

process. Focusing on the heat affected zone, we observe that the hardness slowly decreases as the base material approaches the welding material.

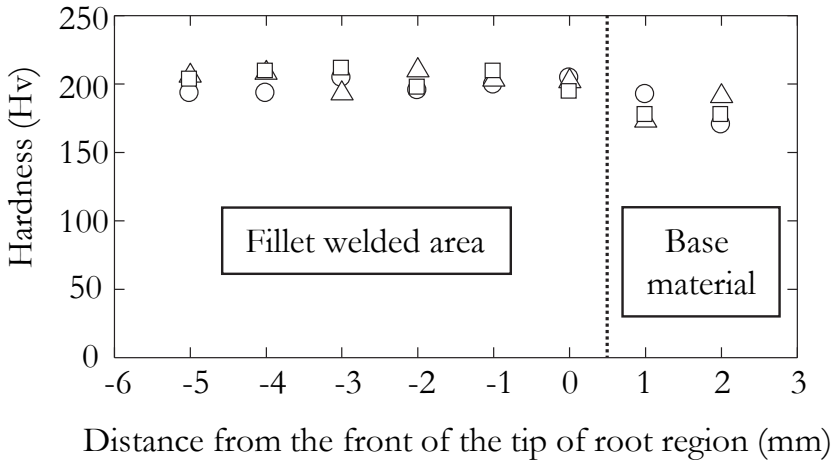

Figure 7: Hardness distribution from the edge of fillet weld.

Fatigue testing results

The fatigue test results are plotted in Fig. 8. The vertical and horizontal axes indicate the amplitude of the force applied to the test piece, and the number of cycles to failure, respectively. Apart from *F*a=7kN, which exhibits widely spread lifetimes, the dispersion of the S-N curve is small. At *F*a=5kN, the lifetime extends to 10^7cycles.

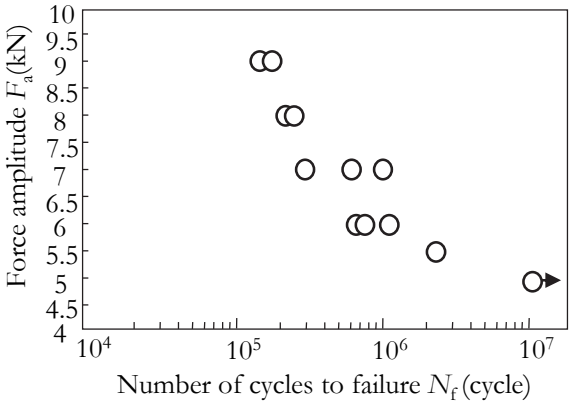

Figure 8: F_a-N curve.

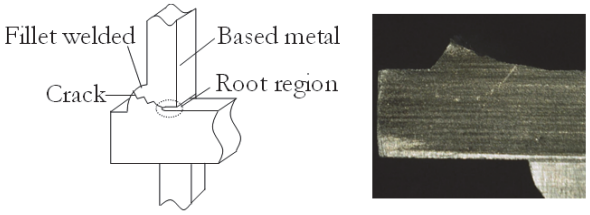

Figure 9: Location of the root region and fracture aspect.

Macroscopic fracture morphology and fractographic study result

We observed the macroscopic fracture morphology of all fractured test pieces. A representative sample is presented in Fig. 9. This piece was tested at *F*a=6kN and observed from the side. The crack was initiated in the unwelded portion and propagated under the welding material at a small angle from the load perpendicular, eventually leading to breakage. The macroscopic fracture morphology and the angle of crack propagation are independent of load under load amplitude. Fig. 10 shows the macroscopic morphology viewed vertically to the load under load amplitudes of *F*a=9, 8, 7, and 6kN. The number of cycles to failure is stated above each image. Many welding defects of various sizes appear in the test pieces. However, the sizes and numbers of the welding defects are unrelated to the number of cycles to failure. Later, we will also demonstrate that crack initiation and propagation is insensitive to the welding defects around the unwelded portion. The details of fracture were examined under a scanning electron microscope (SEM) (Hitachi, Ltd S-3000N). Fig. 11 shows representative SEM images of fractures under a load amplitude of 6kN. Typical fatigue fractures spread over a wide area (panel (b) of Fig. 11), and the ductile fracture extends to 5mm from the tip of the unwelded portion (panel (d)). According to the macroscopic and microscopic observations, cracks are initiated at the tip of the welding defect, and propagate 5mm into the welding material leading to final fracture.

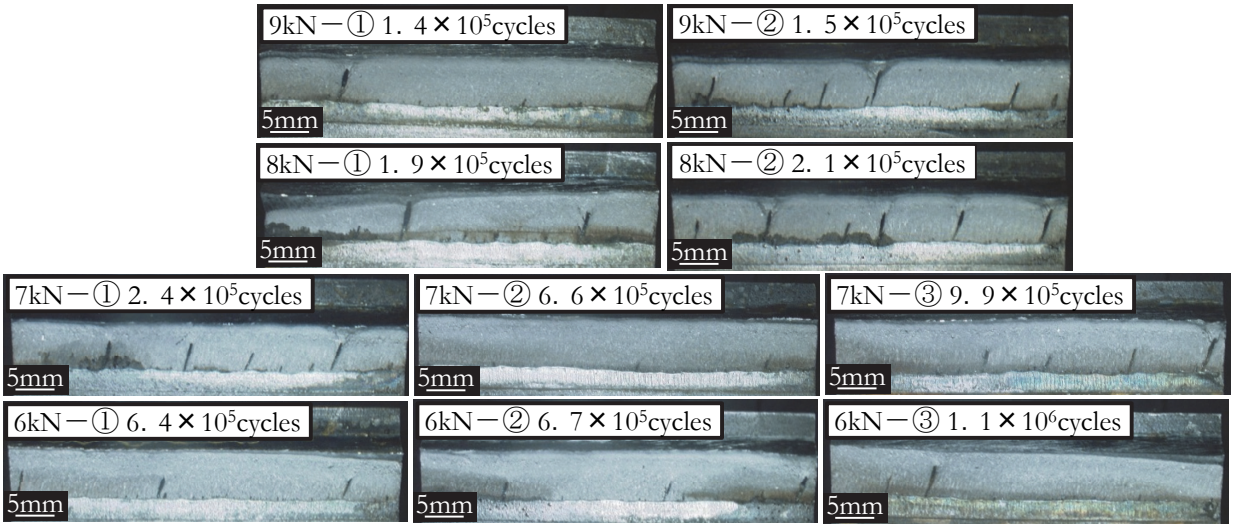

Figure 10: Macro observation.

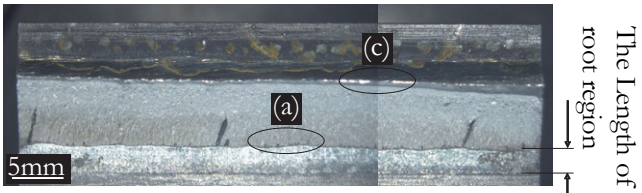

(A) Macroscopic fracture surface of Fa=6kN

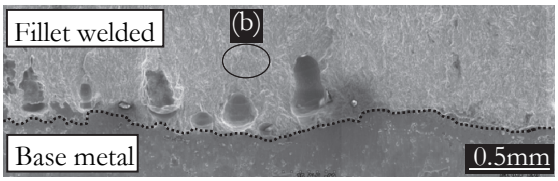

(a) Fatigue fracture surface

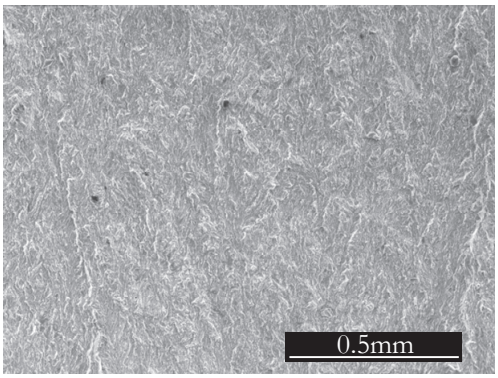

(b) Fatigue fracture surface

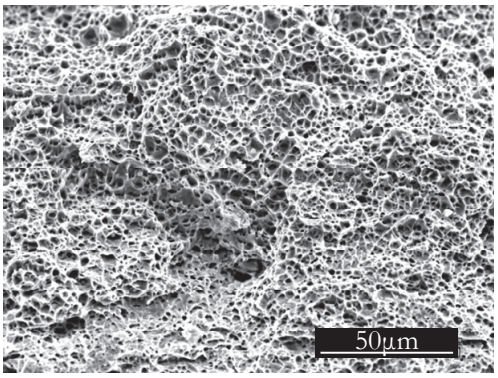

(d) Ductile fracture surface

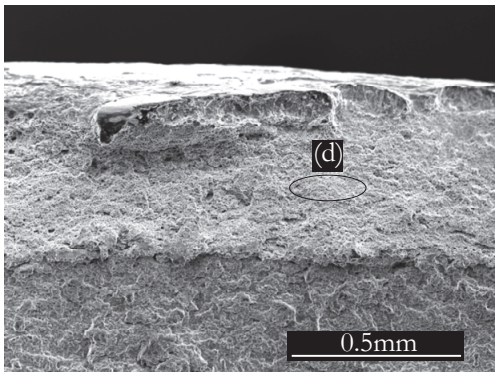

(c) Ductile fracture surface

Figure 11: Microscopic fracture surface.

Observation of crack initiation behavior

In this subsection, we consider the influence of welding defects on fatigue crack initiation and propagation behavior by observing the crack from the root tip of the unwelded portion. The observation results for part of the unwelded portion are presented in Figs. 12 and 13. These images were captured under a load amplitude of 9kN. The test was terminated before it had gone to completion, and the test piece was cut axially to the load and observed near the unwelded portion.

Figs. 12 and 13 show different sections of the same test piece. The test was stopped after 8×10^3 cycles (the longest life N_f at this load amplitude was 1.6×10^5 cycles (N/N_f=5%)).
As in the previous macro observations, the fatigue crack in Fig. 12 initiates at the tip of the unwelded portion and propagates through the welding material. As already mentioned, fatigue crack propagates at some angle from the vertical load axis. However, tiny cracks appearing immediately after the main crack propagate along the vertical load axis. Large welding defects near the unwelded portion, (Fig. 13) exert much less influence on fatigue crack initiation behavior than small defects, because the fatigue crack begins from the root tip of the unwelded portion.

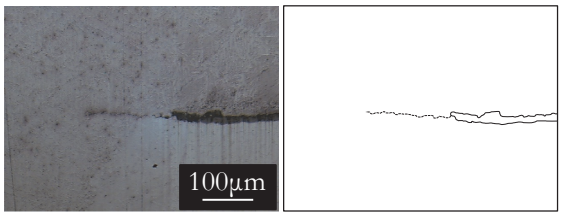

Figure 12: Crack propagation from tip of root region.

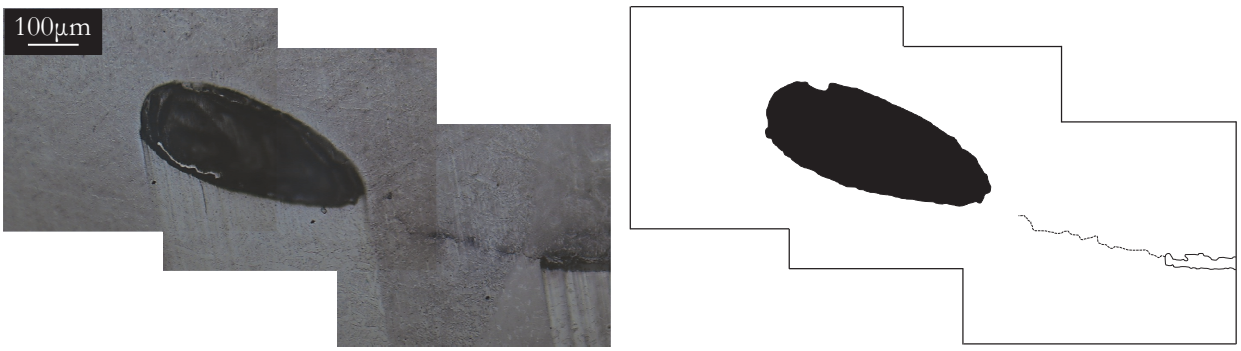

Figure 13: Crack propagation from tip of root region with welding defect.

Crack propagation behavior

In this subsection, we investigate how the fatigue crack propagates into the welding material. Crack propagation behavior from the tip of the unwelded portion is difficult to observe in one-side welded joints such as the present test piece. Thus, we observe fatigue crack by a special three-dimensional observation method, which provides a detailed picture of the fatigue crack propagating into the welding material. The observation method is described below.
First we estimate the fracture lifetime N_f of the test piece, then run a fatigue test up to x% of the estimated lifetime cycles. Next, we grind one side of the test piece, etch it, and acquire images under a light microscope. The surface is ground to 300 – 500μm in the welding direction, and welding photographs are taken from the side. By repeating this process many times in the welding direction, we compile the images into three-dimensional pictures using three-dimensional construction software. Observations were performed under a low and high test force (Fa=6kN and Fa=9kN, respectively), and a three-dimensional picture was compiled in each case. The fracture life N_f under each test force was assumed as the longest lifetime obtained in the fatigue test. (N_f=1.1×10^6 and 1.6×10^5 cycles for Fa=6 and 9kN, respectively). The three-dimensional pictures compiled from repeated grinding, etching and observation under 6 and 9kN loads are shown in Figs. 14 and 15, respectively. Both figures show the crack propagation at three stages of the fracture lifetime: 5, 25, and 50% N_f. The figures are scaled such that the propagating direction is 30 times larger than the width direction (welding direction) of the test piece.
We first investigated the crack aspect at 5% of the estimated fracture lifetime (panel (a) in Figs. 14 and 15). At both force amplitudes, there are cracks extending 0.01 - 0.3 mm across the width of the sample (50mm). This indicates that cracks initiate at a very early stage of the estimated rupture life N_f. It is suggested that the lifetime of crack propagation chiefly determines the fatigue lifetime, and that fatigue crack propagation is very relevant when evaluating fatigue damage in fracture mechanics experiments. At 25% of the estimated fracture lifetime, fatigue damage has progressed (panel (b) of Figs. 14 and 15), and the early stage cracks have propagated into the welding material. The leading edge of the crack is straight and lacks any loose semi elliptical forms, but exhibits protuberance into the crack propagation direction, developing complex overlapping convexities. At 50% of the fracture lifetime, more fatigue damage is evident (panel (c) of

Figs. 14 and 15), but the overall patterns do not evolve, and the leading edge of the crack maintains its complex shape. These observations indicate that multiple cracks initiated at multiple origins coalesce as they propagate, eventually causing complete fracture. The three-dimensional crack observation method cannot provide a continuous picture of the fatigue crack propagation behavior. Therefore, we investigate the leading edge from several crack initiation origins using the beach mark method. In the beach mark test, the load amplitude was Fa=6kN, and the results are shown in Fig. 16. The beach mark was repeated at regular intervals, and the fracture accompanying the crack leading edge was clarified. Fig. 16 also presents a schematic of the crack leading edge emanating from the fracture, and the number of cycles to failure. The N_f of this test piece was 3.5×10^6 cycles. This continuous observation of the crack leading edge by beach marks revealed multiple crack initiation origins, and coalescence of the multiple cracks as the number of cycles increased. From the three-dimensional and beach mark observation results, we confirm that the combination of fatigue cracks plays an important role in fatigue damage, and should therefore be considered in the fatigue mechanics. Fig. 17 is a three-dimensional picture compiled at a load amplitude of 5kN, where the test piece survives to N=10^7cycles. Even at this low force level, there are fatigue crack initiations and crack propagations.

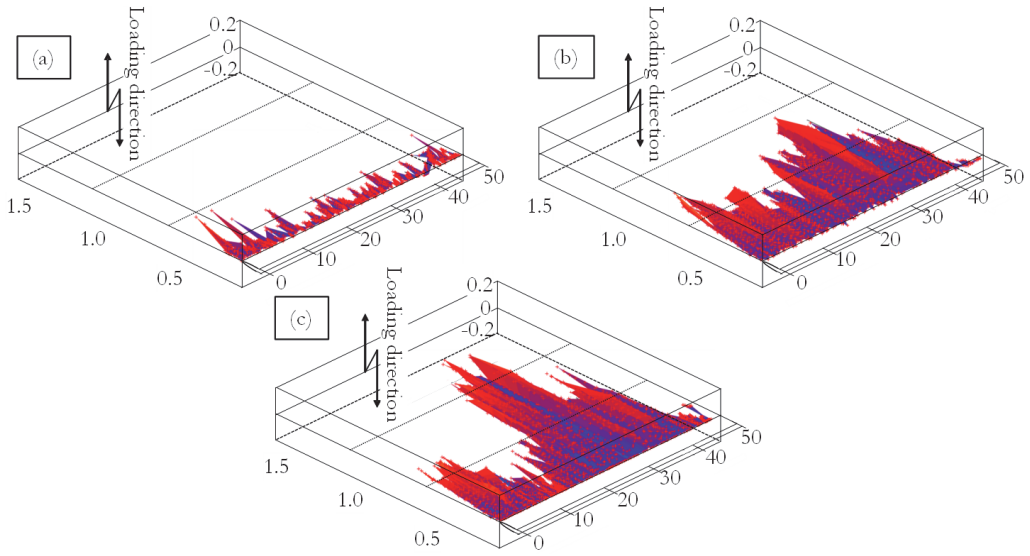

Figure 14: 3-dimentional observation of fatigue crack propagation at the root region (F_a=6 kN).

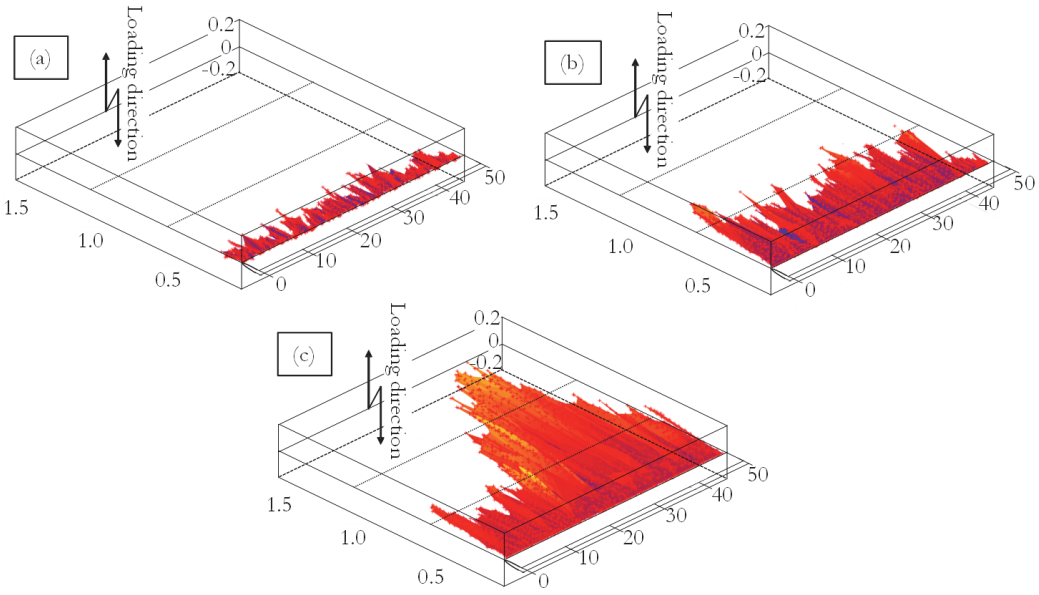

Figure 15: 3-dimentional observation of fatigue crack propagation at the root region (F_a=9 kN).

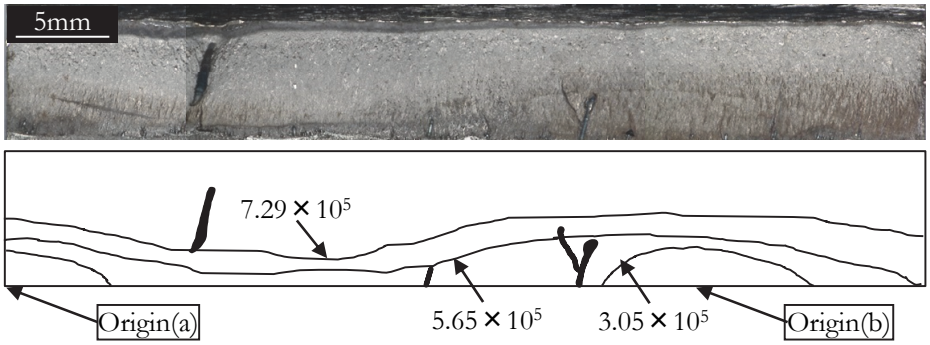

Figure 16: Beach mark on fracture surface of Fa=6kN.

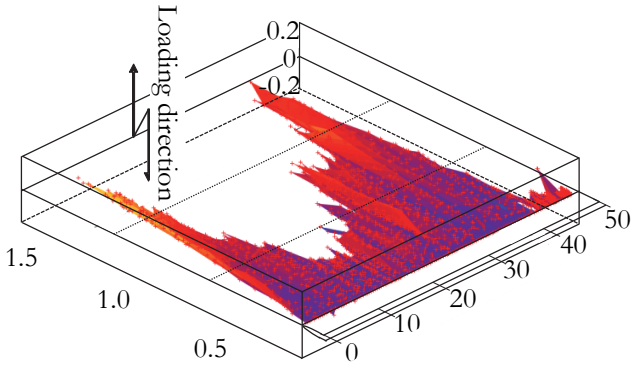

Figure 17: 3-dimentional observation of fatigue crack propagation at the root region (F_a=5 kN, N=10^7cycles).

Relation between crack initiation origin and the shape of the unwelded portion

The above observations confirmed that multiple crack origins occur in the loaded test piece. In this subsection, we consider the location of these crack origins with regard to the shape of the unwelded portion.

As a quantitative evaluation index we define the root gap as the distance from 10μm opposite the crack propagation direction in the unwelded portion. The relationship between root gap and position across the sample width is plotted in Fig. 18. Typical observations of the unwelded portion are presented in Fig.19.

The root gap in the unwelded portion is typically 0.02 - 0.03mm (see circles labeled (b) and (d) in Fig. 18), but multiple narrow gaps in the unwelded portion are also observed (enclosed by circles (a) and (c) in Fig. 18). This unwelded sharp portion may be the origin of a fatigue crack.

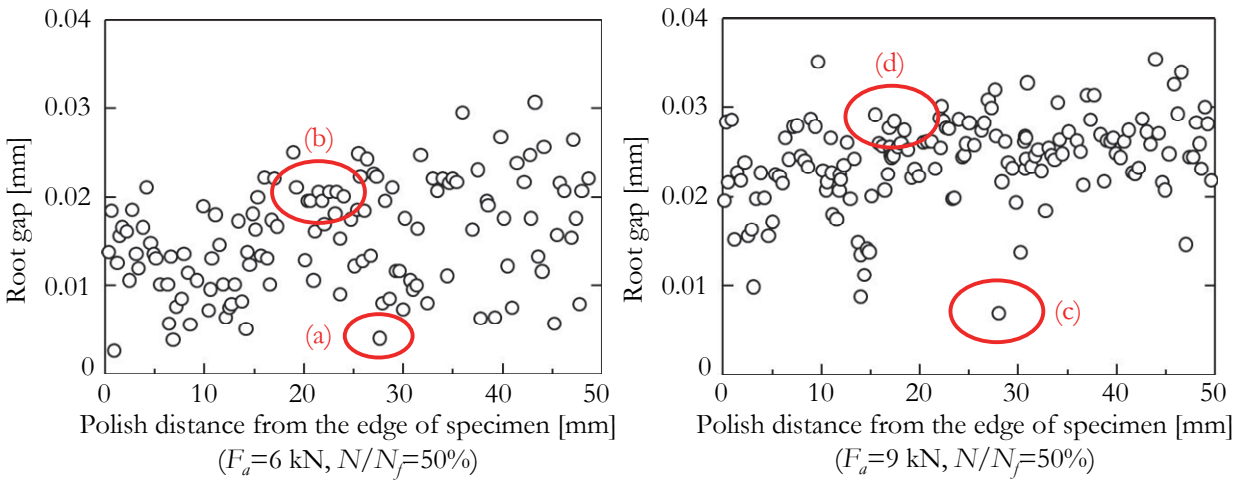

Figure 18: Measurement of the root gap.

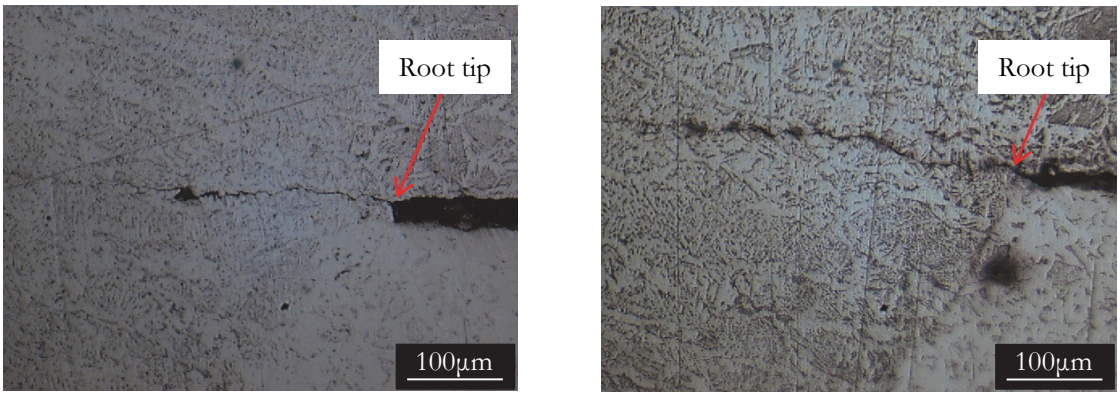

(a) Root tip (b) Narrow root tip

Figure 19: Position of the strain gauge near fillet weld.

CONCLUSIONS

This study, observed crack initiation in a machine piece with one-sided welding of the fillet joints, and crack propagation into the welding material. The aim was to clarify the fatigue properties of the fillet weld and fatigue fracture. Our conclusions are summarized below.

1. Fatigue cracks in the test piece initiated from the tip of the unwelded portion and propagated into the welding materials, eventually leading to fracture. Macro fracture was independent of load amplitude.
2. Multiple welding defects were observed in the unwelded portion, but did not appear to be crack origins. Although these welding defects affected the direction of crack propagation, they exerted minimal influence.
3. The three-dimensional observations revealed that fatigue cracks initiate at an early stage of the fatigue development, and persist throughout the lifetime. We infer that the fatigue lifetime is chiefly governed by the crack propagation lifetime.
4. Cracks were initiated at multiple sites in the test piece. As the number of cycles increased, these cracks propagated and combined.
5. Considering the combination of cracks from multiple crack origins is important for a precise evaluation of fatigue damage.

REFERENCES

[1] Bell, R., Vosikovsky, O., Bain, S. A., The significance of weld toe undercuts in the fatigue of steel plate T-joints, International Journal of Fatigue, 11(1) (1989) 3-11.
[2] Carpinteri, A., Brighenti, R., Huth, H., Vantadori, S., Fatigue growth of surface crack in a welded T-joint, International Journal of Fatigue, 27 (2005) 59-69.
[3] Chung, H.Y., Liu, S.H., Lin, R.S., Ju, S.H., Assessment of stress intensity factors for load-carrying fillet welded cruciform joints using a digital camera, International Journal of Fatigue, 30 (2008) 1861-1872.
[4] Japanese Society of Steel Construction ed., Fatigue design recommendations for steel structures, Japanese Society of Steel Construction.
[5] Kainuma, S., Mori, T., A fatigue strength evaluation method for load-carrying fillet welded cruciform joints, International Journal of Fatigue, 28 (2006) 864-872.
[6] Kanvinde, A.M., Gomez, I.R., Roberts, M., Fell, B.V., Grondin, G.Y., Strength and ductility of fillet welds with transverse root notch, Journal of Constructional Steel Research, 65 (2009) 948-958.
[7] Miki, C., Tateishi, K., Fan, H., Tanaka, M., Fatigue strengths of fillet-welded joints containing root discontinuities, International Journal of Fatigue, 15 (2) (1993) 133-140.
[8] Mori, T., Influence of weld penetration on fatigue strength of single-sided fillet welded joints, Journal of Construction Steel of JSSC, 10(40) (2003) 9–15.

[9] Mori, T., Kainuma, S., A fatigue strength evaluation method for load-carrying fillet welded cruciform joints, Journal of Structural Mechanics and Earthquake Engineering, I-29 (1994) 95-102.
[10] Nakagomi, T., Okada, T., Gun, L., Kubota, K., Experimental study on fatigue strength of cruciform welded joint, Steel construction engineering, 2.
[11] Otegui, J.L., Mohaupt, U.H., Burns, D.J., Effect of weld process on early growth of fatigue cracks in steel T joints, International Journal of Fatigue, 13(1) (1991) 45-58.
[12] The Japan Welding Engineering Society ed., Welding Engineering Standard, The Japan Welding Engineering Society.
[13] Yamada, K., KIM, I., Ito, K., Fatigue behavior of inclined non-load-carrying fillet welded joints, Journal of Structural Mechanics and Earthquake Engineering (I), 682 (I) 56.